The charge density map and electronic band structure of A15-type Cr calculated by the FLAPW method

1995 J. Phys.: Condens. Matter 7 3699

(http://iopscience.iop.org/0953-8984/7/19/004)

J. Phys.: Condens. Matter 7 (1995) 3699–3708. Printed in the UK

The charge density map and electronic band structure of A15-type Cr calculated by the FLAPW method

H Ishibashi, A Yanase and K Nakahigashi

College of Integrated Arts and Sciences, University of Osaka Prefecture, Sakai, Osaka 593, Japan

Received 9 December 1994, in final form 27 February 1995

Abstract. The charge density and electronic band structure of A15-type Cr have been calculated using a self-consistent full-potential linearized augmented plane wave (FLAPW) method. The calculated charge density maps qualitatively reproduce well the maps obtained by a combination of the powder x-ray diffraction data and the maximum-entropy method (MEM). Both charge density maps show the covalent bonding charge between the adjacent 6c site Cr atoms within the infinite linear chain.

The 3d bands are split into the bonding and antibonding states and the density of states exhibits a minimum near the Fermi level of 0.7461 Ryd. The valence electrons occupy only the bonding 3d bands and therefore it seems that the A15-type Cr is a stable structure from the viewpoint of the band structure. The results of the band structure are consistent with the facts that A15-type Cr shows a temperature-independent paramagnetism down to 77 K, and does not have a high superconducting transition temperature which A_3B compounds with the A15-type structure have.

1. Introduction

Since a new modification of Cr with an A15-type structure was discovered by Kimoto and Nishida [1], only a few studies have been made. The reason is that a single phase of the A15-type Cr is not available and usually the phase coexists with a BCC Cr. Consequently, the main investigation of this substance hitherto reported was based on electron microscopy and electron diffraction [2–4] except for a measurement of the magnetic properties [5]. The following three main physical properties were reported:

(1) A15-type Cr is a metastable phase which is easily transformed to a BCC Cr above 450 °C,

(2) this phase is found only in fine particles or thin films and

(3) the fine particles of A15-type Cr show a temperature-independent paramagnetism [5].

Therefore, the other physical properties for the A15-type Cr remain unknown.

Recently, the present authors and colleagues have obtained the electron density distribution of A15-type Cr at room temperature by a combination of powder x-ray diffraction data and the maximum-entropy method (MEM) [6]. The results indicate that there exists mainly a strong covalent bond between the neighbouring 6c site Cr atoms. Furthermore, there exists a weak increase of charge density between the 2a site Cr atom and the bonding electron located at the middle point of the neighbouring 6c site Cr atoms. These features were very similar to those reported for the superconducting compound

0953-8984/95/193699+10$19.50

V_3Si examined by Staudenmann *et al* [7]. However, the A15-type Cr does not show any superconducting properties down to 2 K [6].

On the other hand, Turchi *et al* [8] examined theoretically the electronic structure and the stability of A15-type transition metals and alloys using a tight-binding approximation and the recursion method. They reported that the band contribution to the energy favours the A15-type structure for pure metals when the number of d electrons is about four. However, no other theoretical investigations of A15-type Cr are found. In contrast with the case of A15-type Cr, many of the compounds for a formula A_3B with the A15-type structure, such as V_3Si and Nb_3Sn, exhibit high superconducting temperature and have a variety of anomalous physical properties [9] at low temperatures such as a martensitic phase transition, elastic constants, electric resistivity and magnetic susceptibility. Therefore, many theoretical works on the compounds have been done. For example, Klein *et al* [10] have carried out the self-consistent band structure calculations for the A15-type compounds V_3X and Nb_3X, where X = Al, Ga, Si, Ge and Sn, using the augmented plane wave (APW) method. The results of the electronic band structure calculation show that all the compounds have very flat bands near the Fermi energy E_F and this causes a sharp peak in the density of states around E_F. An especially abrupt change in the density of states near E_F was found for V_3Ga, V_3Si and Nb_3Sn, and therefore this fact appears to be closely correlated with the high superconducting transition temperature and other anomalous physical properties at low temperature. Furthermore, Pickett *et al* [11, 12] have calculated electronic properties of Nb_3Ge, Nb_3Al and hypothetical Nb_3Nb and Nb_3 (chain only) with A15-type structure by the self-consistent pseudopotential method. The results indicate that the Fermi energy lies in a region of very flat bands and that a bonding character along Nb chains, and further B atoms played an important role in determining the electronic structure. The calculated electron charge distribution indicated that the bonding was mainly metallic in character with some covalent-like bonding between the neighbouring Nb atoms.

In the present study, we present the results of the electronic charge density and band structure of A15-type Cr calculated by the full-potential linearized augmented plane wave (FLAPW) method. The calculated charge densities are compared with those of experimental ones. Furthermore some expected physical properties from the calculated energy band structure are discussed.

2. Method of calculation

A self-consistent FLAPW calculation has been carried out to obtain the charge density and the band structure. The exchange and correlation of electrons are taken into account by the local density approximation in the form proposed by Moruzzi *et al* [13]. In the self-consistent calculation, the spin–orbit interactions were included in a perturbative way [14].

The crystal structure of A15-type Cr is shown in figure 1. The space group is $Pm\bar{3}n$ (O_h^3) and each unit cell contains the eight Cr atoms located at positions as follows

Cr(1) 2a site (0, 0, 0), $(\frac{1}{2}, \frac{1}{2}, \frac{1}{2})$
Cr(2) 6c site $(\frac{1}{4}, 0, \frac{1}{2})$, $(\frac{1}{2}, \frac{1}{4}, 0)$, $(0, \frac{1}{2}, \frac{1}{4})$
$(\frac{3}{4}, 0, \frac{1}{2})$, $(\frac{1}{2}, \frac{3}{4}, 0)$, $(0, \frac{1}{2}, \frac{3}{4})$.

The lattice parameter a used in the calculation is 4.600 89 Å [6]. The muffin tin (MT) sphere radii are taken as $0.24a$ on both Cr(1) and Cr(2) atoms, which is a slightly smaller value than that of the maximum possible radii ($a/4$) for Cr(1) atoms. The total MT spheres occupy 46% of the unit cell volume. In the present calculation, we treated the $^{10}Ne + 3s^2$

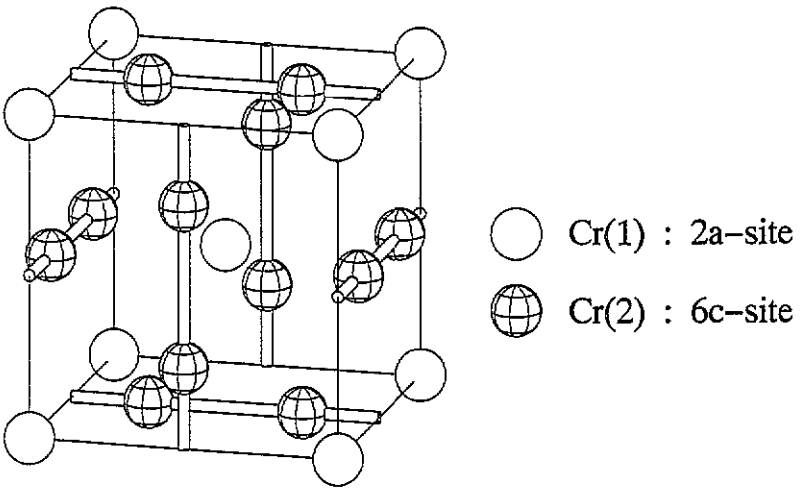

Figure 1. The crystal structure of A15-type Cr.

states for every Cr atom as core electrons. The $3p^6$ states are treated as band electrons using a second energy window. Inside the muffin tin (MT) spheres, the wave functions were expanded in terms of spherical harmonics with the angular momentum $l \leqslant 7$. For the charge densities and potential, the angular momentum expansion is truncated for $l > 6$. The effect of this truncation on the band structure is insignificant because the changes of the energy at the symmetry points were less than 0.001 Ryd when the truncation changed $l > 4$ into $l > 6$. The APW functions with the wave vector $|\boldsymbol{k} + \boldsymbol{G}| = K_{\max} < 5.0(2\pi/a)$, where $\boldsymbol{k}$ is a wave vector in the Brillouin zone (BZ) and $\boldsymbol{G}$ a reciprocal lattice vector, are used in the calculation. The number of APW used was about 500. When $K_{\max}$ increased from $4.5(2\pi/a)$ to $5.0(2\pi/a)$, the changes of the eigenvalues at the symmetry points are less than 0.006 Ryd, and especially less than 0.003 Ryd in the vicinity of the Fermi level.

The self-consistent charge densities and potential have been obtained from the calculated FLAPW wave functions at 35 $\boldsymbol{k}$ points which are uniformly distributed in the irreducible BZ. After the self-consistent calculations, the final band structure is obtained from the energy eigenstates at 286 $\boldsymbol{k}$ points, which are corresponding to a division by 10 of the Γ–X line, in the $\frac{1}{48}$ irreducible BZ. The density of states is determined directly from the above eigenstates using the tetrahedral method [15, 16].

3. Results and discussion

3.1. Charge density map

The contour map of the total charge density obtained in the present calculation for the (001) plane is shown in figure 2, where the 2×2 unit cells are drawn to exhibit the bonding character clearly. Hereafter, we call this the FLAPW map. From this map, the covalent bonding charge is clearly found between the two Cr(2) atoms along the infinite linear chain. The height of the electron density at the midpoint between the adjacent Cr(2) atoms is 0.51 e Å^{-3}. On the other hand, the charge about the Cr(1) atom indicates nearly spherical distribution; however, it slightly spreads out towards the centre of the adjacent Cr(2) atoms.

The electron density distribution map of the (001) plane determined experimentally [6] is shown in figure 3 with the same contour levels as shown in figure 2 for the purpose of

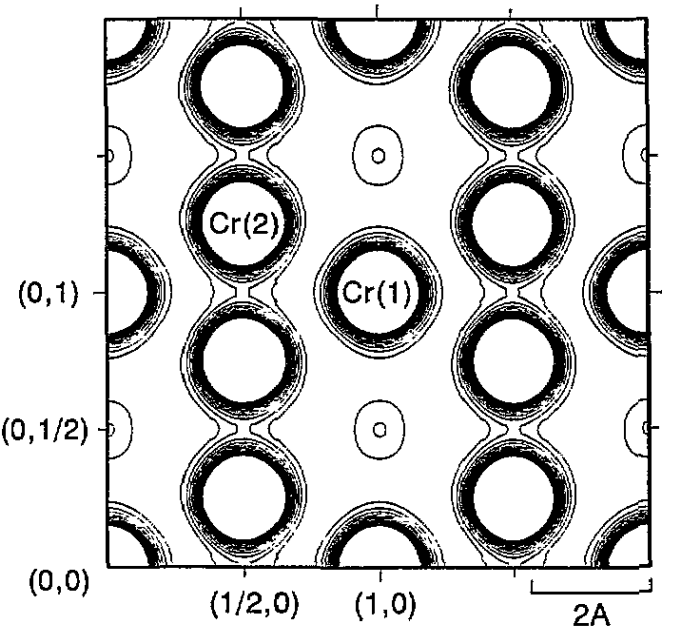

Figure 2. The calculated charge density map (FLAPW map) for the (001) plane of A15-type Cr. The contour lines (e $Å^{-3}$) are drawn from 0.4 to 2.0 with 0.1 intervals.

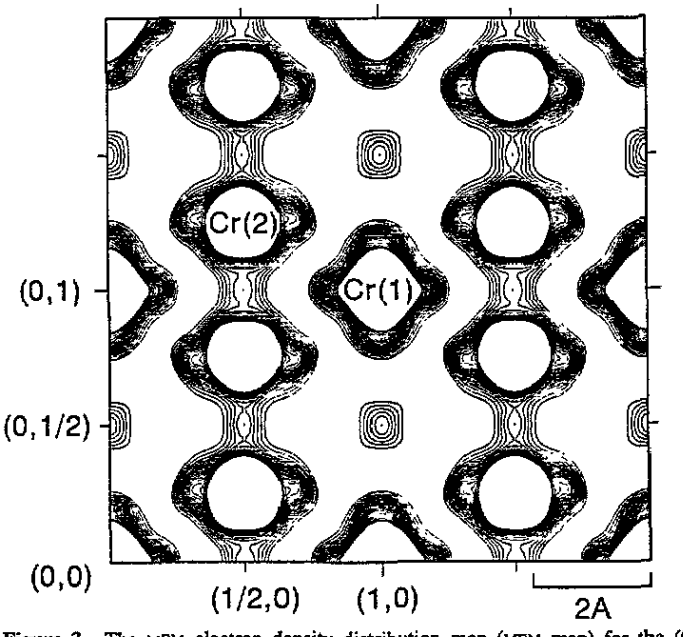

Figure 3. The MEM electron density distribution map (MEM map) for the (001) plane. The contour lines are the same as in figure 2.

comparing with the map obtained in the present calculation. This map has been obtained by powder x-ray diffraction data and the maximum-entropy method (MEM), and hereafter we call this the MEM map. As is clear from figure 3, the MEM map shows the presence of the tight covalent bond between the adjacent Cr(2) atoms. With regard to this feature,

the FLAPW map is in qualitative agreement with the MEM map. However, there are some quantitative differences between the two maps. For example, the MEM map indicates a higher accumulation of electrons along the chains of Cr(2) atoms than the FLAPW map. In practice, the peak height of 0.90 e $Å^{-3}$ at the middle point between the two adjacent Cr(2) atoms in the MEM map is about twice as large as that of the FLAPW map (0.51 e $Å^{-3}$) . Furthermore, both electron density maps show the non-spherical distribution about the Cr(1)atom, which is spread towards the centre of the Cr(2)–Cr(2) bonds, while asphericity in the FLAPW map is much weaker than that in the MEM map. As a result, it seems a weak interaction between the Cr(1) atom and the Cr(2)–Cr(2) bond exists in the ground state. However, a significant difference between the two maps is observed around the Cr(2) atoms. In the MEM map, the electron density about the Cr(2) atoms is spread towards the direction perpendicular to the infinite linear chain, while the FLAPW map shows no indication of such a spread as in the MEM density distribution. The differences between the two maps as described above are probably caused by the anisotropic thermal vibration, because the MEM map has been obtained using data at room temperature, whereas the FLAPW map is based on the ground state.

There was one main difference in the electron density distribution between Nb_3X (X = Ge, Al) calculated by Ho *et al* [12] and the present Cr. In the Nb_3X, there existed two piles of d electrons along the Nb chains forming a 'double hump' between atoms on the chains; however the calculated and observed electron density distributions of the A15-type Cr change rather continuously, making a small maximum at the middle point between the neighbouring Cr atoms though common infinite linear chains existed between the neighbouring Cr or Nb atoms. This may be due to the differences between the d electrons of Nb and Cr. Ho *et al* [12] suggested the 4d electrons caused the 'double-hump' structure; however, in the case of Cr, there exist only the 3d electrons which are much more localized than the 4d electrons. Therefore, small piles possibly occur much nearer the core though these do not appear in figure 2.

Table 1. The calculated structure factors (F_{FLAPW}) and the observed ones (F_{obs}), where the values of the 432 and 520 reflections are calculated from the MEM electron density. The values of F_{obs} were converted to the values taking no account of the thermal vibration effect.

h k l	F_{FLAPW}	F_{obs}
2 0 0	69.22	70.96(19)
2 1 0	−65.51	−67.10(17)
2 1 1	62.61	64.17(16)
2 2 2	−50.88	−50.83(16)
3 2 0	49.67	49.46(14)
3 2 1	48.18	48.25(13)
4 0 0	92.12	90.92(26)
4 2 0	41.91	41.24(12)
4 2 1	−41.09	−40.19(11)
3 3 2	40.20	39.62(12)
5 2 0	36.05	36.13
4 3 2	35.83	38.84
5 2 1	35.53	35.26(10)
4 4 0	68.96	69.12(20)

We have calculated the structure factors F_{FLAPW} from the charge density, and the result is tabulated in table 1 together with the observed ones F_{obs}. In order to compare the

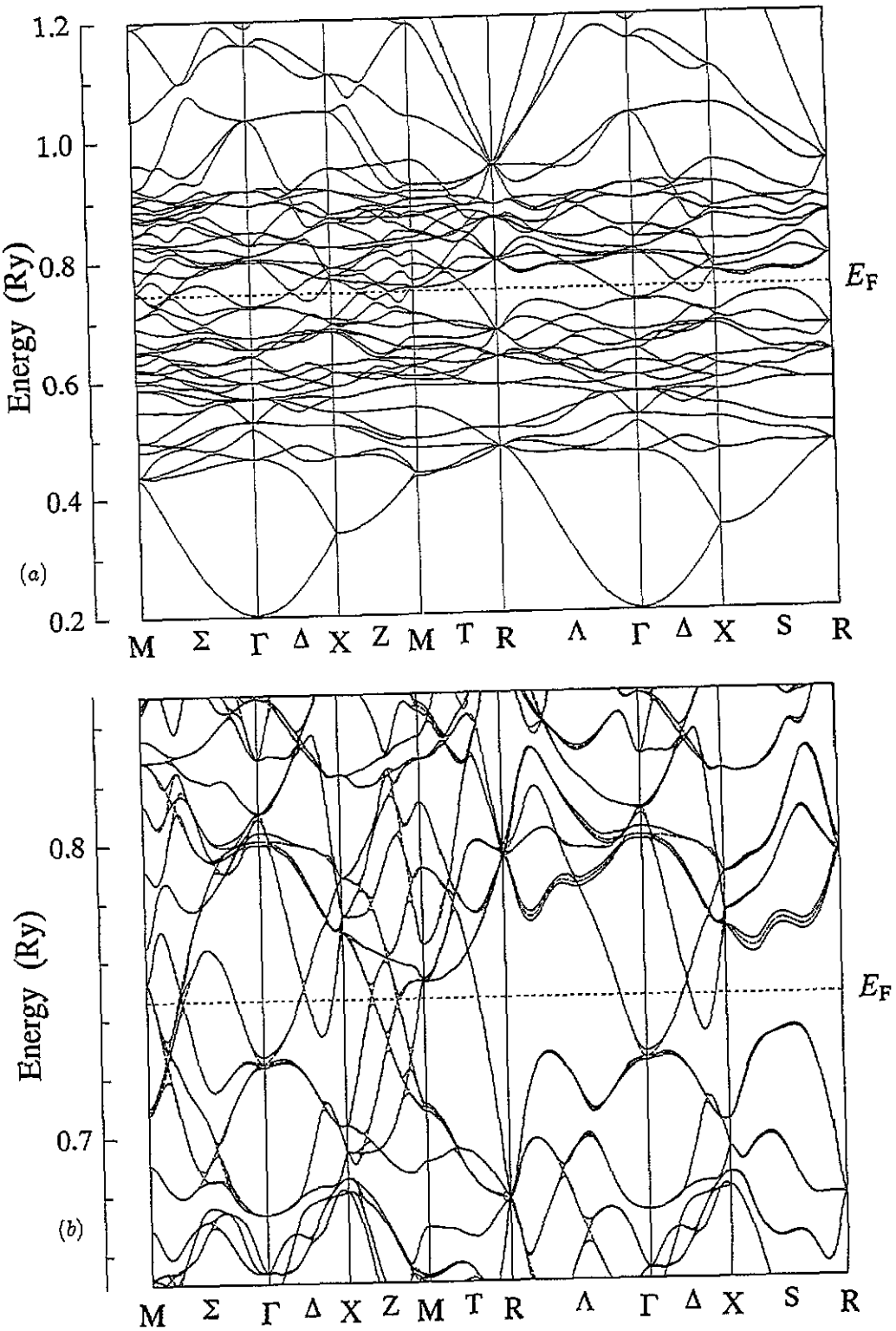

Figure 4. FLAPW band structure of A15-type Cr along the symmetry axes (a) in a wide range and (b) near the Fermi energy. The dashed lines in (b) show the energy bands disregarding the spin–orbit interactions.

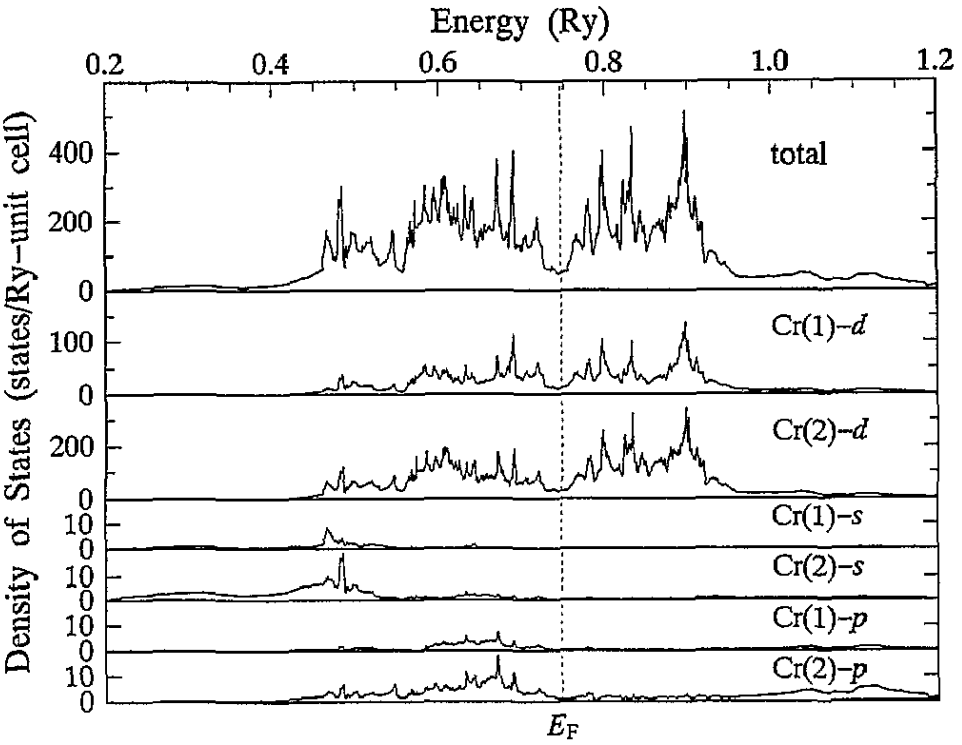

Figure 5. The total and partial density of states for A15-type Cr.

calculated and observed structure factors directly, the values of the observed structure factor are converted to those taking no account of the thermal vibration effect. In the table, the observed structure factors for the 432 and 520 reflections are calculated from the MEM electron density because it is impossible to decompose into the respective integrated intensity from the powder x-ray diffraction intensity data. As is clear from table **1**, the calculated structure factors agreed fairly well with the observed ones except for a few reflections.

3.2. Band structure and density of states

The calculated energy bands along the symmetry axis in a wide energy range and near the Fermi energy are shown in figure 4(a) and 4(b), respectively. In figure 4(b), the band structure without spin–orbit interactions is also shown by the dashed lines in order to exhibit the effect of the interactions. Furthermore, the total and partial density of states are shown in figure 5. The 3p bands are well localized in the narrow range from −2.46 to −2.33 Ryd, and therefore they are not shown in the figures. The Fermi energy E_F, which is indicated by a broken line in figures 4 and 5, is 0.7461 Ryd. Low-lying 4s bands are seen below 0.4 Ryd, and above it, the complex energy bands due to s–p–d hybridization are formed below E_F. However, generally speaking, the narrow 3d bands which appear between 0.4 Ryd and 0.95 Ryd are found in the broad 4s–4p bands. From figure 5, the 3d bands are split into the bonding and antibonding states, and the density of states exhibits a minimum between the two states near E_F. Consequently, A15-type Cr is stable from the point of view of the band structure. The total density of states $N(E_F)$ at the Fermi level was 56.18 (states Ryd^{-1}/unit

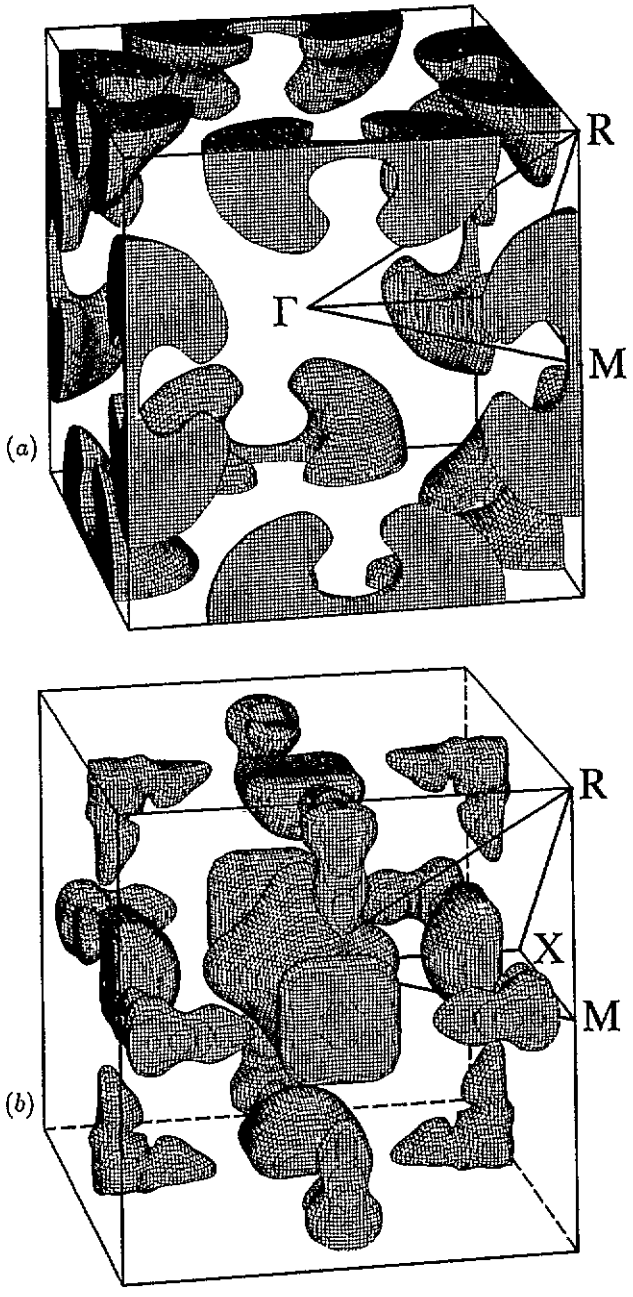

Figure 6. (a) Hole Fermi surface of A15-type Cr derived from the 24th band. (b) Electron Fermi surface derived from the 25th band.

cell).

On the other hand, many theoretical studies on the band structure for BCC Cr have been reported. For example, Laurent *et al* [17] calculated the band structure of a paramagnetic BCC Cr by the linear combination of Gaussian orbitals (LCGO) method. The densities of states for the two structures resemble each other in their characteristic features. However, the total density of states per atom of A15-type Cr is somewhat smaller than that of BCC Cr. The value was 7.02 and 9.14 (states Ryd^{-1}) for A15-type and BCC Cr, respectively.

In the present calculation, spin–orbit interactions are taken into account; however, all bands have twofold degeneracy due to the time reversal symmetry because A15-type Cr has inversion symmetry. Thus these two bands are counted as one. From figure 4(b), it is found that many bands are split by the spin–orbit interactions. All bands along the S axis have twofold degeneracy when the spin–orbit interactions are not taken into account; however, these bands are very slightly split by the spin–orbit interactions except for the bands a little above E_F, in which the splitting is clearly seen. Furthermore, accidental degeneracy appears in the bands along the Δ, Z and Σ axes when the spin–orbit interactions are not considered. However, the degeneracies are broken by the spin–orbit interactions. As a result, energy gaps appear in the bands along the Δ, Z and Σ axes near E_F. These gaps affect the Fermi surface, namely the spin–orbit interactions severely affect the shape of the Fermi surface. In this structure, a characteristic feature occurs at the R point, i.e. both bands at 0.678 Ryd and 0.796 Ryd in figure 4(b) have sixfold degeneracy. When the spin–orbit interactions are considered, each band is slightly split into two bands with fourfold and twofold degeneracy. Consequently, this many-fold degeneracy causes the larger density of states near the energy levels at the R point. In practice, the sharp structures in the density of states appear near the energy level of 0.68 Ryd and 0.80 Ryd as shown in figure 5. The E_F is located near the middle level between the two energy levels at the R point, thus the density of states $N(E_F)$ at E_F has a small value and a nearly flat structure near E_F.

The band structure of the A_3B compounds with A15-type structure was calculated by Klein *et al* [10] and Pickett *et al* [11] using the APW and the self-consistent pseudopotential method, respectively. All the calculated band structures are very similar to the result for the present Cr. Of course, the bands at the R point of the A_3B compounds have many-fold degeneracy, thus the density of states has a large value near such an energy level because these compounds have the same crystal structure as A15-type Cr. However, E_F is located near the energy level at the R point in the case of the A_3B compounds. Furthermore, the flat bands around the Γ point exist near E_F for V_3Ga, V_3Si, Nb_3Sn, Nb_3Ge and Nb_3Al. Pickett *et al* indicated that the calculated d states are split into bonding and antibonding bands separated by a small gap just above E_F. However the bonding d bands are flatter than the antibonding bands and therefore the density of states $N(E)$ has an extremely spiky structure in the region below E_F. This spiky structure of the A_3B compounds corresponds to that near the peak at the energy level near 0.68 Ryd in figure 5 for A15-type Cr. However, the E_F of A15-type Cr is located far from such an energy level because the number of valence electrons of Cr is larger than that of the A atom (V or Nb) in A_3B compounds. It is believed that the spiky structure in the density of states causes the high superconducting transition temperature and anomalous physical properties. The density of states of Nb_3Ge and Nb_3Al is about four times as large as that of the A15-type Cr. Pickett *et al* suggested that Nb_3Nb will not be a very high-temperature superconductor even when this substance is stabilized because of its comparatively small value of $N(E_F)$. However, the calculated value of $N(E_F)$ of Nb_3Nb is twice as large as that of the present A15-type Cr. Therefore, A15-type Cr is not expected to be a superconducting substance. In practice, A15-type Cr does not show superconductivity down to 2 K.

The 24th and 25th bands in figure 4(b) cross the Fermi level and cause the Fermi surface. The occupancies per unit cell of the 24th and 25th bands are 1.780 and 0.220, respectively. Figure 6 shows Fermi surfaces for holes and electrons of A15-type Cr. The hole Fermi surface derived from the 24th band is a closed one whose shape is like twin mushrooms joined at the M point as shown in figure 6(a). The 25th band produces three kinds of closed electron Fermi surface, which have a slightly deformed octahedral shape centred at the Γ point, a pillow-shaped one on the Δ axis and a boot-shaped one near the M point, respectively as shown in figure 6(b). The pillow surface has a fairly flat part perpendicular to the Δ axis. The distance between the two flat parts is about $0.13(2\pi/a)$. These facts possibly cause the magnetic ordering such as the spin density wave. However, this ordering may arise at extremely low temperature because the flat area is very small. In practice, A15-type Cr does not exhibit such a magnetic ordering, i.e. it shows a temperature-independent paramagnetism down to 77 K [5].

References

[1] Kimoto K and Nishida I 1967 *J. Phys. Soc. Japan* **22** 744–56
[2] Forssell J and Persson B 1969 *J. Phys. Soc. Japan* **27** 1368–9
[3] Forssell J and Persson B 1970 *J. Phys. Soc. Japan* **29** 1532–45
[4] Nishida I and Kimoto K 1974 *Thin Solid Films* **23** 179–89
[5] Matsuo S, Nishida I, Kimoto K and Noguchi S 1978 *J. Phys. Soc. Japan* **44** 1387–8
[6] Ishibashi H, Arita M, Nishida I, Yanase A and Nakahigashi K 1994 *J. Phys.: Condens. Matter* **6** 8681–90
[7] Staudenmann J L, Coppens P and Muller J 1976 *Solid State Commun.* **19** 629–33
[8] Turchi P, Treglia G and Ducastelle F 1983 *J. Phys. F: Met. Phys.* **13** 2543–67
[9] Testardi L R 1975 *Rev. Mod. Phys.* **47** 637–48
[10] Klein B M, Boyer L L, Papaconstantopoulos D A and Mattheiss L F 1978 *Phys. Rev.* **18** 6411–38
[11] Pickett W E, Ho K M and Cohen M L 1979 *Phys. Rev.* B **15** 1734–50
[12] Ho K M, Pickett W E and Cohen M L 1979 *Phys. Rev.* B **15** 1751–61
[13] Moruzzi V L, Janak J F and Williams A R 1978 *Calculated Electron Properties of Metals* (Oxford: Pergamon)
[14] Takeda T and Kubler J 1979 *J. Phys. F: Met. Phys.* **9** 661–72
[15] Jepson O and Anderson O K 1971 *Solid State Commun.* **9** 1763–7
[16] Rath J and Freeman A J 1975 *Phys. Rev.* B **11** 2109–17
[17] Laurent D G, Callaway J, Fry J L and Brener N E 1981 *Phys. Rev.* B **23** 4977–87